This is the accepted version of the publication Zhao Q, Zhang D, Liu J, et al. Generalized degradation model and bond failure analysis of pultruded basalt/carbon/glass FRP bars and profiles in concrete environments. Advances in Structural Engineering. 2025;0(0). Copyright © 2025 (The Author(s)). DOI: 10.1177/10963480221081781.

Generalized Degradation Model and Bond Failure Analysis of Pultruded

2 Basalt/Carbon/Glass FRP Bars and Profiles in Concrete Environments

- 3 Qi Zhao¹; Daxu Zhang²; Jie Liu³; Keitai Iwama⁴; Pei-Fu Zhang² Lingxin Zeng⁵; Xiao-Ling Zhao^{1,6*}
- 4 Department of Civil and Environmental Engineering, The Hong Kong Polytechnic University, Hong Kong, China;
- 5 Email: qi-cn.zhao@polyu.edu.hk (Qi Zhao)
- 6 ² State Key Laboratory of Ocean Engineering, Shanghai Key Laboratory for Digital Maintenance of Buildings and
- 7 Infrastructure, School of Ocean & Civil Engineering, Shanghai Jiao Tong University, Shanghai, China; Email:
- 8 daxu.zhang@sjtu.edu.cn (Daxu Zhang); peifu.zhang@sjtu.edu.cn (Pei-Fu Zhang)
- 9 ³ College of Civil Engineering, Nanjing Forestry University, Nanjing, China; Email: <u>Jieliu@outlook.com</u>;
- 10 ⁴ Institute for Multidisciplinary Sciences, Yokohama National University, Yokohama, Japan; Email: <u>iwama-keitai-</u>
- 11 <u>ft@ynu.ac.jp</u> (K. Iwama);
- 12 ⁵ School of Civil Engineering and Transportation, North China University of Water Resources and Electric Power,
- 13 Zhengzhou, China; Email: zenglingxin@ncwu.edu.cn
- 14 ⁶ Research Institute of Land and Space, The Hong Kong Polytechnic University, Hong Kong, China
- 15 Xiao-Ling Zhao (Corresponding author): xiao-lin.zhao@polyu.edu.hk

16 **Highlights:**

- Damage mechanisms of polymer matrices and fibers are summarized and classified.
- A physically based degradation model is proposed and validated by test data.
- The generalized degradation model is applicable to pultruded FRP bars, tubes, and sections.
- A bond failure criterion for the deterioration evaluation of pultruded FRP bars is provided.

Abstract: In this paper, the degradation mechanisms of pultruded fiber-reinforced polymer (FRP) composites with various types of fibers and polymer matrices, including basalt, carbon, and glass fibers, as well as amine-cured and anhydride-cured epoxy matrices, styrene-cured vinyl ester matrices, and unsaturated polyester matrices, are summarized under corrosive environments. Then, the damage mechanisms of the components of pultruded FRP composites are classified into three groups, including chemical etching & leaching, hydrolysis, and physical degradation. Additionally, a generally degradation model, the hydroxyl ions diffusion-based model (HIDM), is proposed and validated using extensive test data, demonstrating good accuracy and wide applicability for pultruded FRP composites with various cross-sectional shapes. The structural safety of FRP-reinforced concrete structures will be significantly weakened when the damage depth became greater than 6% diameter of FRP bars, corresponding to a strength retention of 77.4%. Furthermore, a new bond failure criterion for pultruded FRP bars used in construction, damage depth level, is proposed to evaluate the premature deterioration and functional obsolescence of FRP-reinforced concrete structures, which could provide a unique perspective and insight for structural safety assessment.

- 35 **Keywords:** FRP composites; degradation mechanisms; fibers; polymer matrix; degradation analysis;
- 36 concrete environment;

21

22

23

24

25

26

27

28

29

30

31

32

33

34

37

1 Introduction

Fiber-reinforced polymer (FRP) composites have been successfully applied in the aviation, military, and automotive industries. In recent decades, they have gradually been adopted as reinforcement materials for concrete structures to prevent premature deterioration caused by steel corrosion (Zhao et al., 2019). Unlike steels, FRP composites are corrosion-resistant in environments rich in chloride salts, which can lead to severe depassivation and rusting of steel reinforcements embedded in concrete. Since the 1990s, there have been numerous successful applications of FRP-reinforced concrete structure in construction, including bridge decks and girders, seawalls, ports, and docks (Gooranorimi and Nanni, 2017; Li et al., 2019). The durability of FRP reinforcements in concrete is widely concerned by engineers. To evaluate the FRP degradation in concrete, accelerated tests are widely performed by exposing them to harsh environments, such as seawater, wet-dry cycles, and simulated concrete/seawater sea-sand concrete pore solutions. Based on these accelerated tests, researchers have proposed several empirical and semiempirical degradation models, as illustrated in Fig. 1. These models provide good predictions under their respective exposure conditions. However, various types of concrete have been developed for construction by using different types of mixing water (e.g., water and seawater), cement/cementitious admixture (e.g., Potland cement, fly ash, silica fume, Ground granulated blast-furnace slag), and fine/coarse aggregates (e.g., river sands, sea sands, gravel, coral or recycled aggregates) (Dhondy et al., 2021; Teng et al., 2019; Yang et al., 2022; Zhang et al., 2022a; Zhou et al., 2021). Naturally, the microstructures and internal environments (e.g., pore structures, moisture content and alkalinity) in these concrete vary, significantly affecting the long-term performance of FRP reinforcements embedded in these concrete (Bazli et al., 2021; Li et al., 2021). Therefore, the available models based on empirical equation or regression analysis from specific experimental data, lack the ability to offer a universal methodology for predicting the degradation of FRP composites under various service conditions. To address this issue, it is necessary to establish a physically based generalized model for

evaluating the deterioration of pultruded FRP composites in various concrete.

42

43

44

45

46

47

48

49

50

51

52

53

54

55

56

57

58

59

60

61

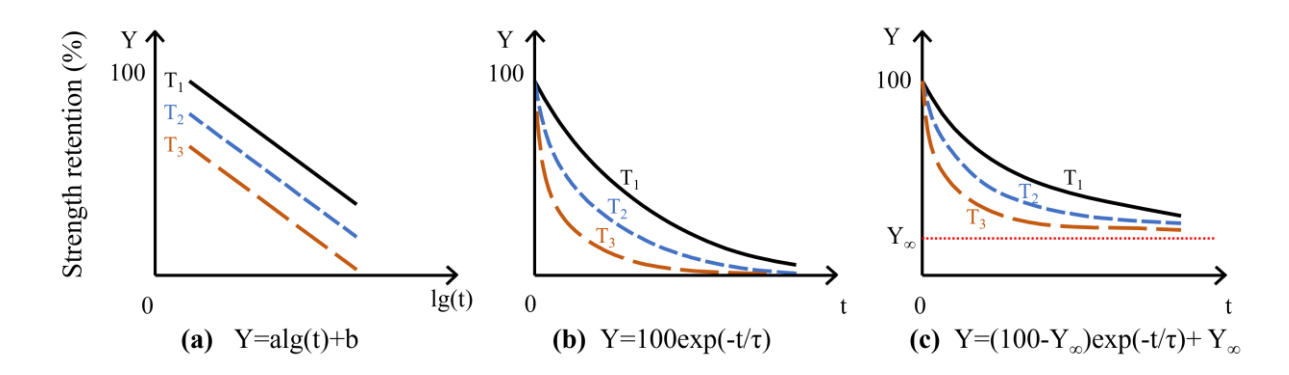


Fig. 1 Common degradation models of FRP composites (Adapted from (Wang, Zhao, Xian, Wu, Singh Raman, Al-Saadi, et al., 2017))

64

65

66

67

68

69

70

71

72

73

74

75

76

77

78

79

80

On the other hand, the FRP-to-concrete bond strength is fragile to the surface degradation of the pultruded FRP bars either embedded in concrete or adhered to concrete, such as bars, tubes and sections (Liu et al., 2024; Sun et al., 2021). Extensive researches have been conducted to evaluate the FRP-toconcrete bond strength (Benmokrane et al., 2020; Liao et al., 2022; Taha and Alnahhal, 2021; Zhang et al., 2024a). These studies demonstrated that the bond strength could be affected by various parameters including the compressive and splitting tensile strength of concrete, effective bond length, FRP stiffness, surface treatment of FRP, rib spacing, and rib height (Lu et al., 2021; Shrestha et al., 2015). However, the FRP-to-concrete bond degradation are mainly determined by the durability and surface damage depth of FRP due to long-term exposure to the environment (ACI Committee 440, 2015, 2017; Allen and Atadero, 2012; CEN/TS 19101, 2022; Liu et al., 2022; Ortiz et al., 2023). This is because the high alkalinity in concrete can cause the degradation of FRP reinforcements as the exposure period increased (Zhao et al., 2021, 2022, 2024a, 2024b). However, the coupled effects of long-term exposure to various service environments on pultruded FRP in construction are usually considered using the environmental reduction factors or conversion factors by the current codes (Benmokrane et al., 2020; Ceroni et al., 2018; Correia et al., 2023; Myers and Viswanath, 2006; Zhang,

et al., 2022). These factors are, in essence, to reserve an adequate safety redundancy for FRP-reinforced/-strengthened concrete structures during the design service life. No definite variables are available to calculate the damage as service time increases (Huang and Aboutaha, 2010). Hence, it is necessary to propose a definite time-dependent variable for the pultruded FRP bar-to-concrete bond strength degradation.

In this paper, the damage mechanisms of polymer matrices and fibers for various types of pultruded FRP composites are summarized and classified. Then, based on their damage mechanisms, a generalized degradation model is proposed and validated using extensive test data, demonstrating good accuracy and applicability for various types of pultruded FRP composites, such as bars, laminates, plates and tubes. Additionally, a new bond failure criteria is proposed and discussed, providing a unique perspective and insight to the long-term durability considerations for the current design guidelines.

2 Theory and Methodology

2.1 Damage mechanisms of FRP in concrete environments

FRP composites typically consist of fibers, matrices, and fiber-matrix interfaces. Accordingly, the damage mechanisms of FRP composites can be classified into three types based on their chemical composition: degradation of glass, basalt, and carbon fibers; polymer matrices (i.e., polyester, epoxy, and vinyl ester); and the fiber-matrix interfaces.

The chemical constituents of glass fiber primarily include SiO₂, Al₂O₃, CaO, and MgO, with minor components such as ZrO₂, Na₂O, and K₂O, each comprising less than 1% by weight. Previous studies (Chen et al., 2006, 2007; Wang et al., 2017a, 2017b; Wu et al., 2015; Zhao et al., 2021, 2022, 2024)

have shown that glass fibers can be etched by hydroxyl ions. Free hydroxyl ions in solutions can react with the crystal Si-O-Si in glass fibers and generate silanol (-SiOH), a loose gel which facilitates water absorption and subsequent chemical attacks (Du et al., 2024; Guo et al., 2022; Zhao, Zhang, Zhang, et al., 2025; Zhao, Zhang, Zhao, et al., 2025), as described by Eqs. (1) - (3).

Basalt fibers have similar chemical compositions with glass fibers but with varying weight fractions and the addition of FeO. The presence of FeO in basalt fibers compromises their durability in concrete pore solutions (Kaushik and Islam, 1995; Mehta and Monteiro, 2014). Surface degradation occurs when chloride ions (Cl⁻) and oxygen (O₂) arrive at the fiber surface and react with iron ions, forming rust (Kaushik and Islam, 1995; Mehta and Monteiro, 2014), as shown in Eqs. (4) - (6). However, carbon fibers are inert in concrete environments (i.e., alkaline or salt-alkaline pore solutions) due to their stable chemical structure, consisting of stacks of turbostratic carbon layers (Peebles, 2018).

Polyester, epoxy, and vinyl ester matrices are commonly used in FRP applications. Polyester matrices can be hydrolyzed in alkaline solutions because their ester groups are vulnerable to hydroxyl ions (Chin et al., 2001; Kootsookos and Mouritz, 2004). Similarly, the ester groups in the cross-linking nodes of epoxy matrices, cured by aliphatic or aromatic anhydrides, are also susceptible to hydrolysis. Although the cross-linking nodes in styrene-cured vinyl matrices are generally inert, the vinyl ester resin itself contains ester groups that are prone to hydrolysis in alkaline environments, as described in Eq. (7) (Zhao et al., 2021; Zhao, X Zhao, et al., 2024).

The fiber-matrix interfaces of pultruded FRP composites for construction, are typically made of coupling agents (i.e., siloxane) designed to bond fibers and matrices together, allowing polymer matrices to transfer loads to fibers efficiently. The degradation mechanism of siloxane (Si-O-C) in

concrete pore solutions is similar to that of glass fibers due to the presence of -Si-O-Si-O-C structures (Zhao, X Zhao, et al., 2024).

In summary, glass and basalt fibers primarily will degrade due to chemical etching and leaching in concrete pore solutions, while carbon fibers remain inert in these environments. The curing agents used also have significant influence on the degradation of polymer matrices. Polyester and anhydride-cured epoxy matrices are fragile to hydrolysis in alkaline environment (Sembokuya et al., 2003), whereas amine-cured epoxy matrices exhibit better corrosion resistance but can still absorb water due to the extensive hydrophilic groups in their cross-linked network, e.g., the amine (-CONH) and ether (-O-) bonds (Fang and Guo, 2023; Gao et al., 2020; Tanks et al., 2022), leading to swelling-induced physical degradations (Hojo et al., 1991; Lim et al., 2019) and slow hydrolysis at high temperatures (Fang and Guo, 2023; Hojo et al., 1998). Besides, recent studies have reported that hydrophilic groups in amine-cured epoxy resins may become cleavable sites when exposed to adverse environments, such as ultraviolet radiation (Brand et al., 2020; Long et al., 2023; Ma et al., 2017).

Table 1 Damage mechanisms of pultruded FRP composites in concrete environments

FRP components	Exposure conditions	Damage mechanisms	Eq.	Refs
Glass fiber	Alkaline solution	$Si - O(Na) + H_2O \rightarrow SiOH + Na^+ + OH^-$	(1)	(Chen et al., 2006, 2007; Wang,
Basalt fiber	or	$Si-O-Si+OH^- \to SiOH+Si-O^-$	(2)	Zhao, Xian, Wu, Singh Raman
Interface	salt-alkaline solution	$Si-O^-+H_2O\to SiOH+OH^-$	(3)	and Al-Saadi, 2017; Wang, Zhao,
(siloxane)				Xian, Wu, Singh Raman, Al-
				Saadi, et al., 2017; Wu et al.,
				2015; Zhao et al., 2021, 2022;
				Zhao, X Zhao, et al., 2024)
Basalt fiber	Salt solution	$Fe^{2+} + Cl^- \rightarrow [FeCl\ complex]^-$	(4)	(Kaushik and Islam, 1995; Mehta
	or	$[FeCl\ complex]^- + OH^- \rightarrow Fe(OH)_2 + Cl^-$	(5)	and Monteiro, 2014)
	Salt-alkaline solution	$Fe(OH)_2 + O_2 + H_2O \rightarrow Fe(OH)_3 \rightarrow Fe_2O_3 \cdot nH_2O$	(6)	
Carbon fiber	Alkaline solution, salt-alkaline	No degradation		(Peebles, 2018)
	solution,			
	or salt solution			

Anhydride-	Alkaline solution	$R'COOR'' + OH^- \rightleftharpoons R'CO^-(OH)OR''$	(7)	(Chin et al., 2001; Kootsookos and
cured epoxy	or	$\rightarrow R'COO^- + R''OH$		Mouritz, 2004; Sembokuya et al.,
Styrene-cured	salt-alkaline solution			2003; Zhao et al., 2021, 2024)
vinyl				
Polyester				
matrix				
Amine-cured	Alkaline solution or salt-	Water uptake and swelling-induced physical		(Arias et al., 2018; Brand et al.,
epoxy	alkaline solution	degradation;		2020; Fang and Guo, 2023; Gao et
		Dissociation of secondary/tertiary amine		al., 2020; Hojo et al., 1998; Long
		R' - NH - R'' and ether $R' - O - R''$ in		et al., 2023; Ma et al., 2017; Tanks
		the amine-cured epoxy		et al., 2022)

Note: the alkaline solution in this table denotes the common concrete environments, while the salt-alkaline solution refers to the marine concrete environments, such as seawater sea-sand concrete pore solution.

2.2 Degradation classifications

The integrity of the polymer matrix is of significance for the service performance of FRP composites. Based on extensive accelerated tests (Arias et al., 2018; Brand et al., 2020; Chen et al., 2006, 2007; Chin et al., 2001; Fang and Guo, 2023; Gao et al., 2020; Hojo et al., 1998; Kaushik and Islam, 1995; Kootsookos and Mouritz, 2004; Long et al., 2023; Ma et al., 2017; Mehta and Monteiro, 2014; Peebles, 2018; Sembokuya et al., 2003; Tanks et al., 2022; Wang, Zhao, Xian, Wu, Singh Raman and Al-Saadi, 2017; Wang, Zhao, Xian, Wu, Singh Raman, Al-Saadi, et al., 2017; Wu et al., 2015; Zhao et al., 2021, 2022; Zhao, X Zhao, et al., 2024), three corrosion types of polymer matrices are concluded: the surface reaction type, corroded-layer-forming type, and penetration type, as illustrated in Fig. 2. The surface reaction occurs when the polymeric matrix comprises simple low molecules in the main chains and cross-links, both bonded by esters, allowing the corroded part to dissolve into the immersed aqueous solutions (Hojo et al., 1991). However, when the polymer skeleton and curing agents are longer and larger, the main polymer chains tangle, retarding the dissolution of decomposed parts, and thus the matrix corrosion shifts from surface reaction to corroded-layer-forming type. The penetration type is

characterized by a two-stage diffusion/reaction behavior: firstly, the environmental solution penetrates the cured resin body until reaching equilibrium, subsequently causing a rapid decrease in mechanical strength. The latter two corrosion types are dominated by the diffusion process and apply to many commonly used polymer matrices, such as aromatic amine-cured epoxy resin and styrene-cured vinyl ester resins. According to our recent study (Zhao et al., 2021, 2022, 2024), the surface reaction type is more applicable to unsaturated polyester-based and aliphatic/alicyclic anhydride-based FRP composites with smaller repeating units of polymer chains.

Unlike tensile strength, the compressive and shear properties of FRP composites are mainly determined by the matrix properties. Any changes in the matrix properties due to increased temperature or moisture absorption will be reflected in these matrix-controlled properties of the composites (Mallick, 2018).

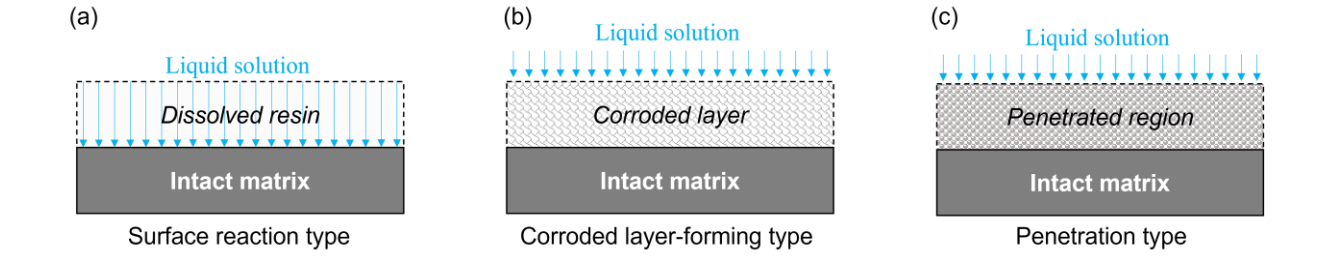


Fig. 2 The corrosion types of polymer matrices (Adapted from (Hojo et al., 1991))

Table 2 Classifications of damage mechanisms of FRP composites

Components of FRP composites	Conditions	Degradation classifications
Glass fibers	Alkaline or salt-alkaline solution for all	Etching & leaching
Basalt fibers	fibers	Etching & leaching
Carbon fibers		No degradation
Anhydride-cured epoxy	Alkaline or salt-alkaline solution for all	Hydrolysis
Amine-cured epoxy	epoxy and resin	Swelling-induced physical degradation & subsequent
		scission of secondary/tertiary amine and ether groups
Styrene-cured vinyl ester resin		Hydrolysis
Unsaturated Polyester matrix		Hydrolysis
Siloxane interface	Alkaline or salt-alkaline solution	Etching

2.3 Generalized degradation model of pultruded FRP composites in concrete environments

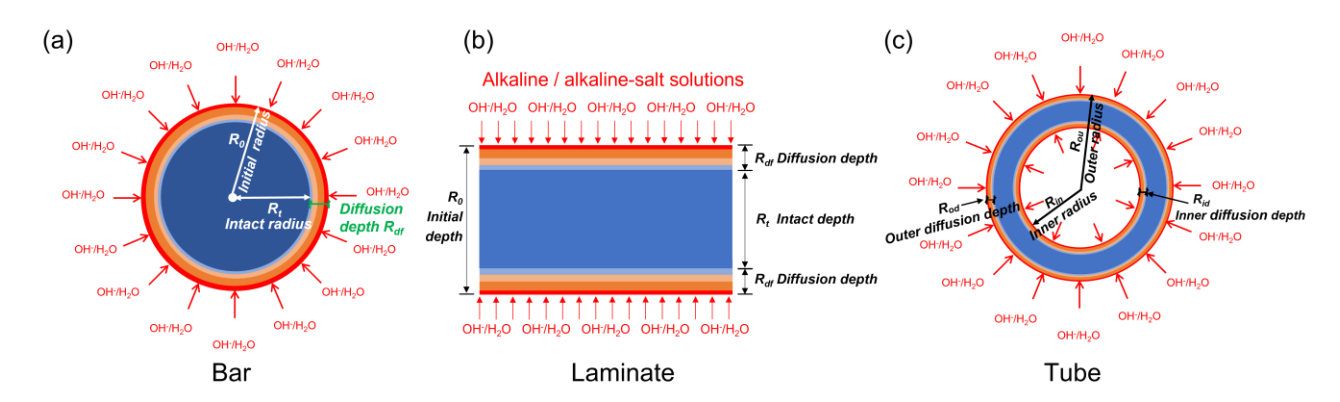


Fig. 3 Schematic of OH- diffusion in the cross-sections of FRP (a) Bar, (b) Laminate (Adapted from Zhao et al.,

Since B/C/GFRP composites are susceptible to hydroxyl ions (OH⁻) in concrete pore solutions, the degradation of FRP composites can be evaluated by examining the OH⁻ distributions in their cross-sections. Consequently, the damage depth of FRP composites can be determined by the threshold value of OH⁻ (Zhao et al., 2021; Zhao, X Zhao, et al., 2024). As verified in Table 2 and Fig. 2, a generalized degradation model, the hydroxyl ions diffusion-based model (HIDM), has been proposed and validated by the authors (Zhao et al., 2021, 2024).

When the concrete pore solutions diffuse into the FRP laminates or plates from one side, as illustrated in Fig. 3(b), the governing equation can be simplified as 1D self-diffusion process, which follows the Fick's second law.

$$\frac{\partial c(x,t)}{\partial t} = D \frac{\partial^2 c(x,t)}{\partial x^2} \tag{8}$$

where c is the OH^- concentration, x is the diffusion depth, and D is the diffusion coefficient. The analytical solution is given as follows (Zhao et al., 2021):

$$c = \frac{c_0}{2} \left[1 - \psi \left(\frac{x}{2\sqrt{Dt}} \right) \right] \tag{9}$$

where $\psi(\frac{x}{2\sqrt{Dt}})$ is the error function, as shown in Eq. (10).

$$\psi\left(\frac{x}{2\sqrt{Dt}}\right) = \frac{2}{\sqrt{\pi}} \int_0^{\frac{x}{2\sqrt{Dt}}} e^{-y^2} \, dy \tag{10}$$

- However, the governing equation regarding the FRP bars or tubes can be described by Eq. (11), as
- illustrated in Fig. 3(a) and 3(c).

$$\frac{\partial c(r,t)}{\partial t} = D\left(\frac{\partial^2 c(r,t)}{\partial r^2} + \frac{1}{r}\frac{\partial c(r,t)}{\partial r}\right) \tag{11}$$

- where r is radial distance from the center, t is exposure time.
- 186 The OH⁻ distribution across the FRP bars is shown by Eq. (12) (Zhao, X Zhao, et al., 2024).

$$c(r,t) = c_s - 2(c_s - c_0) \sum_{n=1}^{\infty} \frac{J_0(\beta_n r)}{\beta_n R_0 J_1(\beta_n R_0)} e^{-D\beta_n^2 t}$$
(12)

- where c_s is OH⁻ concentration at the bar surface; c_0 is the initial concentration; $x_n = \beta_n R_0$ (n=1,
- 188 2, 3 ...) are the zeros of the equation $J_0(x) = 0$.
- The zero-order and one-order Bessel functions of the first kind (J_0, J_1) are shown by Eqs. (13) and
- 190 (14), respectively.

$$J_0(x) = 1 + \frac{(-1)}{2^2 \times (1!)^2} x^2 + \frac{(-1)^2}{2^4 \times (2!)^2} x^4 + \dots + \frac{(-1)^i}{2^{2i} \times (i!)^2} x^{2i} + \dots$$
 (13)

$$J_1(x) = \frac{x}{2} + \frac{(-1)^1}{2^3 \times 2!} x^3 + \frac{(-1)^2}{2^5 \times 2! \times 3!} x^5 + \dots + \frac{(-1)^i}{2^{2i+1} \times i! \times (i+1)!} x^{2i+1} + \dots$$
 (14)

- Eq. (15) describes the relationship between the residual intact depth R_t , diffusion depth R_{df} , and
- initial radius R_0 . The initial strength f_0 and residual strength f_t of FRP composites before and after
- exposure, as shown in Eq. (16). The strength retention equals the

$$R_t = R_0 - R_{df} \tag{15}$$

$$\frac{f_t}{f_0} = \frac{S_t}{S_0} \tag{16}$$

$$R_t = R_0 \sqrt{\frac{f_t}{f_0}} \tag{17}$$

$$\frac{f_t}{f_0} = \frac{R_t}{R_0} \tag{18}$$

$$\frac{f_t}{f_0} = \frac{(R_{ou} - R_{od})^2 - (R_{in} + R_{id})^2}{(R_{ou} - R_{in})^2}$$
(19)

- where S_0 and S_t are the initial cross-sectional area and the residual intact area (e.g., the area marked
- in blue in Figs. 3(a) and 3(c)) of FRP composites before and after exposure, respectively.
- The strength retention of FRP bars after exposure can be calculated using Eq. (17), while Eq. (18)
- can be used to calculate the strength retention for FRP laminates, as illustrated in Fig. 3(b). Eq. (19) is
- applicable to the strength degradation evaluation of FRP tubes under both outer and inner exposure to
- solutions, as shown in Fig. 3(c). The long-term durability of other FRP composites can be assessed
- using Eq. (16) based on their cross-sectional types, such as channel and H-sections.
- According to our recent research (Zhao et al., 2021, 2022; Zhao, X Zhao, et al., 2024; Zhao, X-L
- Zhao, et al., 2024), the diffusion depth R_{df} at the concentration $c(R_{df}, t)$ of 10^{-7} mol/L (pH=7) can
- be assumed as the maximum damage depth, and they agreed well with the experimental data. Besides,
- both the residual tensile strength and interlaminar shear strength (ILSS) of FRP bars which are
- dependent on their cross-sectional areas, conform to the maximum cross-sectional stress criteria (Zhao
- et al., 2021, 2022, 2024). This is because the OH⁻ penetration will reduce the effective bar diameter
- and the cross-sectional areas of bars (also termed as residual cross-sectional area), thus decreasing the
- 208 strength capacity of FRP bars.
- Besides, the diffusion coefficient D at different temperatures can be calculated using Eq. (20)
- 210 (Antoon and Koenig, 1980).

$$D = D_0 \exp\left(-E_{df}/(RT)\right) \tag{20}$$

where D_0 is a constant, E_{df} is the activation energy for diffusion, T is the Kelvin temperature, and

212 R is the universal gas constant.

213

214

215

216

217

218

219

220

221

222

223

224

225

226

227

228

229

230

 D_0 and E_{df} can be determined through the experimental data at two elevated temperatures, then

diffusion coefficients D of FRP composites at other temperatures under concrete pore solutions can

be calculated according to Eq. (20).

2.4 Suggested bond failure criterion for FRP composites embedded in concrete due to corrosion

The initial properties of FRP composites (i.e., the guaranteed tensile strength) usually do not consider the long-term exposure to the environments. In general, concrete structures are designed based on the limit state principles (i.e., ultimate limit state and serviceability limit state) (ACI Committee 440, 2015, 2017). However, the environmental conditions uniquely affect the long-term performance of encased FRP composites in both FRP-reinforced and FRP-strengthened concrete structures. Consequently, decades of exposure to the service environments might change the dominate limit state of concrete members reinforced with FRP bars from ultimate limit state to serviceability limit criteria, especially for those FRP reinforcements that exhibit low stiffness, such as pultruded GFRP and BFRP bars. Regarding the durability considerations for FRP reinforcements, the design strength of FRP bars is used by multiplying an environmental reduction factor, ranging from 0.5 to 1.0 (ACI Committee 440, 2015, 2017). Additionally, current codes adopt the reduced resistance capacity of FRP bar-concrete members by dividing various partial factors γ ranging from 0.6 to 1.0 (CEN/TS 19101, 2022), thus reserving redundant safety for concrete structures. However, the current guides do not present how these factors adopted in design could extend the long-term durability of FRP-concrete structures. Besides, there are no quantitative criteria for the long-term degradation of pultruded FRP bars embedded in concrete. The environmental reduction factor C_E , partial factor γ and conversion factor η_c in the available design guides are listed in Tables 3, 4 and 5.

Table 3 Environmental reduction factors for various fibers, FRP systems and exposure conditions

Exposure conditions	Fiber type	Environmental reduction	Reference
		factor	
		C_E	
Concrete not exposed to earth and weather	Carbon	1.0	(ACI Committee 440, 2015)
	Glass	0.8	
	Aramid	0.9	
Concrete exposed to earth and weather	Carbon	0.9	(ACI Committee 440, 2015)
	Glass	0.7	
	Aramid	0.8	
Interior exposure	Carbon	0.95	(ACI Committee 440, 2017)
	Glass	0.75	
	Aramid	0.85	
Exterior exposure	Carbon	0.85	(ACI Committee 440, 2017)
(Bridges, piers, unenclosed parking garages)	Glass	0.65	
	Aramid	0.75	
Aggressive environment	Carbon	0.85	(ACI Committee 440, 2017)
(Chemical plants, and wastewater treatment plants)	Glass	0.50	
	Aramid	0.70	
Concrete both exposed and not exposed to earth or weather	Glass	0.85	(ACI Committee 440, 2023)

Table 4 Conversion factors η_{cm} for unprotected FRP composite materials and epoxy adhesives

Exposure classes	Conversion factor	Influence of moisture	Reference
	η_{cm}		
I	1.00	Indoor exposure with service temperature according to 1.1(4)	(CEN/TS 19101, 2022)
II	0.85	Outdoor exposure with service temperature according to 1.1(4),	(CEN/TS 19101, 2022)
		without (i) continuous exposure to water, (ii) permanent immersion	
		in water, (iii) permanent exposure to a relative humidity higher than	
		80%, (iv) combined UV-radiation and frequent freeze-thaw cycles	
III	0.60	Continuous exposure to water (or seawater), or permanent	(CEN/TS 19101, 2022)
		immersion in water (or seawater), or permanent exposure to a	
		relative humidity higher than 80% (material temperature up to $25\ensuremath{^\circ C}\xspace)$	

Note: The above conversion factors are applicable to composite materials with glass, carbon or basalt fibers and thermoset polymer matrix of either unsaturated polyester, vinylester or epoxy, and for epoxy adhesives.

242

243

244

245

246

247

248

249

250

251

252

253

254

255

Table 5 Conversion factor for temperature η_{ct} for FRP composite materials

Properties of composite materials	Conversion factor for temperature η_{ct}	Reference
For fiber-dominated properties	$ \eta_{ct} = \min \left\{ 1.0 - 0.25 \cdot \frac{T_s - 20}{T_g - 20}; 1.0 \right\} $	(CEN/TS 19101, 2022)
For matrix-dominated properties	$ \eta_{ct} = \min \left\{ 1.0 - 0.80 \cdot \frac{T_s - 20}{T_g - 20}; 1.0 \right\} $	(CEN/TS 19101, 2022)

Note: T_s is the maximum material temperature in service conditions (in °C); T_g is the glass transition temperature (in °C). And the conversion factor, $\eta_{c=} \eta_{ct} \bullet \eta_{cm}$

To address this ambiguity, it is necessary to establish a definite FRP-to-concrete bond failure criterion to evaluate the service performance of FRP bar-reinforced concrete structures from the perspective of the damage depth of FRP bars. As widely known, the serviceability conditions of FRP bar-reinforced concrete structures depend on the cooperative work between FRP bars and concrete. Hence, it is crucial to maintain good bond strength at the design level to avoid premature failure during the intended service life. However, long-term exposure to concrete environment might degrade the encased FRP bars, and the surface deterioration and an increasing damage depth of FRP bars can be expected during service. Subsequently, the bond strength between concrete and FRP bars/plates will be weakened. When the damage depth increased to a threshold value, B/C/GFRP bars will lose majority of their bond capacity to reinforce or strength concrete. Based on extensive data from published literature, Zhang et al. (Zhang et al., 2024b, 2024c) studied various surface types of FRP bars, including the helically wrapped FRP bars (i.e., Figs.4(a) and 4(b)) and deformed FRP bars (i.e., Figs.4(c) and 4(d)) with different rib height and rib spacing, and concluded that optimal FRP bar-toconcrete bond strength could be achieved when the FRP bars with a rib height of around 6% bar diameter and a rib-spacing-to diameter of 1.0, were adopted, as illustrated in Fig. 4.

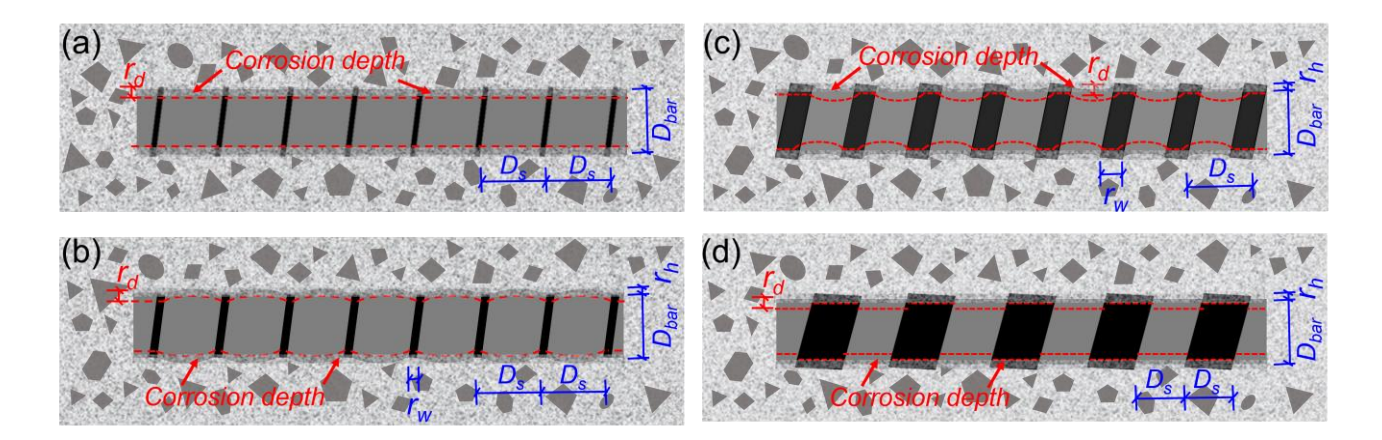


Fig. 4 Surface types of FRP bars and FRP-to-concrete bond degradation

Note: D_{bar} is the diameter of FRP bars, D_s is the rib space; r_w and r_h denote the rib width and rib height of FRP bars, respectively. r_d denotes the critical damage depth.

However, when the ribs and surfaces of FRP bars were corroded, the interfacial frictions and mechanical interlock between concrete and FRP bars will disappear. Subsequently, the interfacial bond strength between FRP bars and concrete cannot be guaranteed, risking the serviceability limit state of FRP bar-concrete structures, as shown in Fig. 4. Herein, the damage depth of 6% bar diameter, corresponding to a strength retention of 77.4%, can be assumed as the threshold value. Therefore, the damage depth of FRP bars embedded in concrete should be less than 6% bar diameter to avoid bond failure. To make this criteria more universal for FRP bars with various diameters, the damage depth level of FRP bars was proposed to evaluate the service performance conditions of FRP bars embedded in concrete during service. The damage depth level was defined as the ratio of the damage depth to the FRP bar diameter (termed as D_{bar}).

3 Validation and discussion

To validate the applicability of HIDM, the experimental data from various types of FRP composites in published literature, including the B/C/GFRP bars, laminates and tubes, were used to compare with

the predicted strengths (Bazli et al., 2020; Wang et al., 2020; Wang, Zhao et al., 2017a, 2017b; Wu et al., 2015). The diffusion coefficients used for the following validation are summarized in the appendix Table A1.

3.1 Pultruded BFRP bars

3.1.1 BFRP bars exposed in common concrete pore solutions

The experimental results from Wu et al. (Wu et al., 2015) were used to validate the effectiveness of HIDM for BFRP bars exposed to common concrete pore solutions. The initial pH value of the concrete pore solution was approximately 13.0. The OH distributions along the radial depth are illustrated in Fig. 5(a). It was observed that OH concentration decreased with increasing depth at temperature of 25°C, 40°C, and 55°C. Furthermore, higher temperatures significantly accelerated the diffusion process of OH, thereby speeding up the degradations of BFRP bars. The predicted tensile strengths agreed well with the experimental results, with a relative error (RE) ranging from 0.4% - 3.7%, as shown in Fig. 5(b). The maximum RE between experimental values and predictions was 3.7%, demonstrating the accuracy of the HIDM.

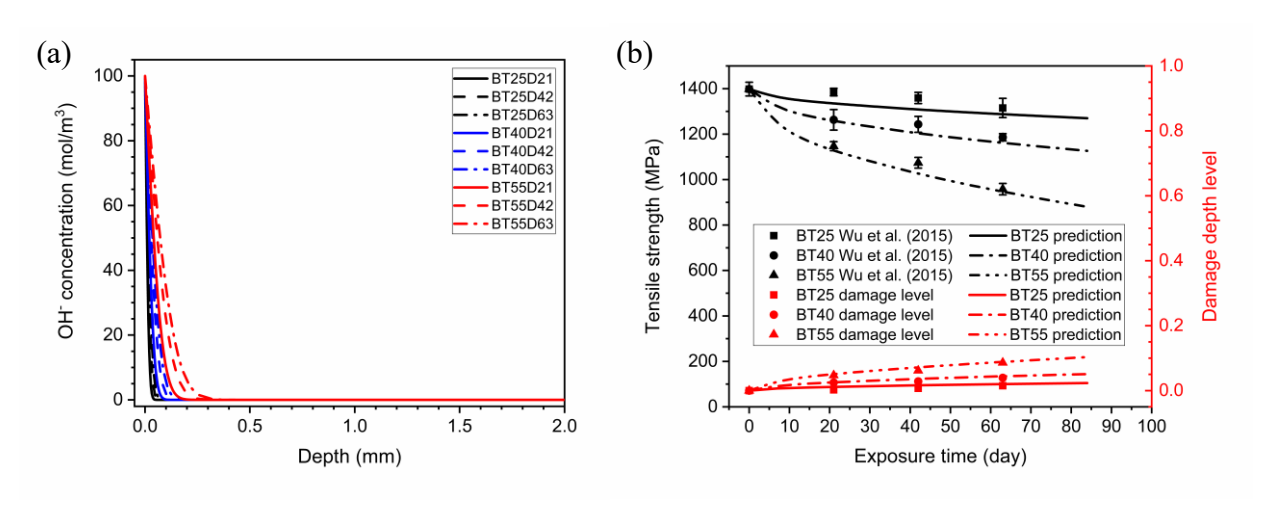


Fig. 5 Predicted results of (a) OH⁻ concentration and (b) tensile strength of BFRP bars in concrete pore solution

Note: BT25D21 represents the conditioned BFRP bars with an exposure period of 21 days at 25°C. B denotes the basalt fiber, T denotes temperature, D denotes the exposure days.

3.1.2 BFRP bars exposed in SWSSC pore solutions

289

290

291

292

293

294

295

296

297

298

299

300

301

302

303

304

305

306

307

308

309

310

311

Comparisons were conducted using experimental results from Wang et al. (Wang et al., 2017b) in both normal concrete (NC) and high-performance (HP) seawater sea-sand concrete (SWSSC) pore solutions. In this experiment, 28 accelerated conditions were employed, including four temperatures (32°C, 40°C, 48°C, 55°C) and four exposure periods (21, 42, 63, 84 days) for the normal SWSSC (NC) environment, and three temperatures (25°C, 40°C, 55°C) and four exposure periods (21, 42, 63, 84 days) for the high-performance SWSSC (HP) environment. The pH values of the NC and HP pore solutions were 13.4 and 12.7, respectively. The OH⁻ distributions along the radial direction were obtained using HIDM, as shown in Figs. 6(a) and 7(a). Subsequently, the tensile strength of BFRP bars under different conditions were calculated, as depicted in Figs. 6(b) and 7(b). Compared to the experimental data under the HP SWSSC pore solutions, the RE of predicted tensile strength varied between 1.1 - 3.6%, 4.2% - 5.4%, and 2.4% - 5.1% for the BFRP bars at 32°C, 40°C, and 55°C, respectively. These predictions were in good accordance with the test results. For the BFRP bars under the NC SWSSC pore solutions, the predictions at 32°C and 40°C were accurate compared to experimental results, as shown in Fig. 6(b). However, there were significant difference between the predicted values and test data at T48D21, T48D42, and T55D21 conditions. This discrepancy can be attributed to the large dispersion at high temperatures, which lead to greater

damage depths and smaller intact core cross-sectional areas. Subsequently, OH- ions can penetrate the residual intact cross-section of FRP bars along the defected regions. In general, the HIDM provides an acceptable evaluation of the long-term mechanical strength of BFRP bars in alkaline or salt-alkaline solutions.

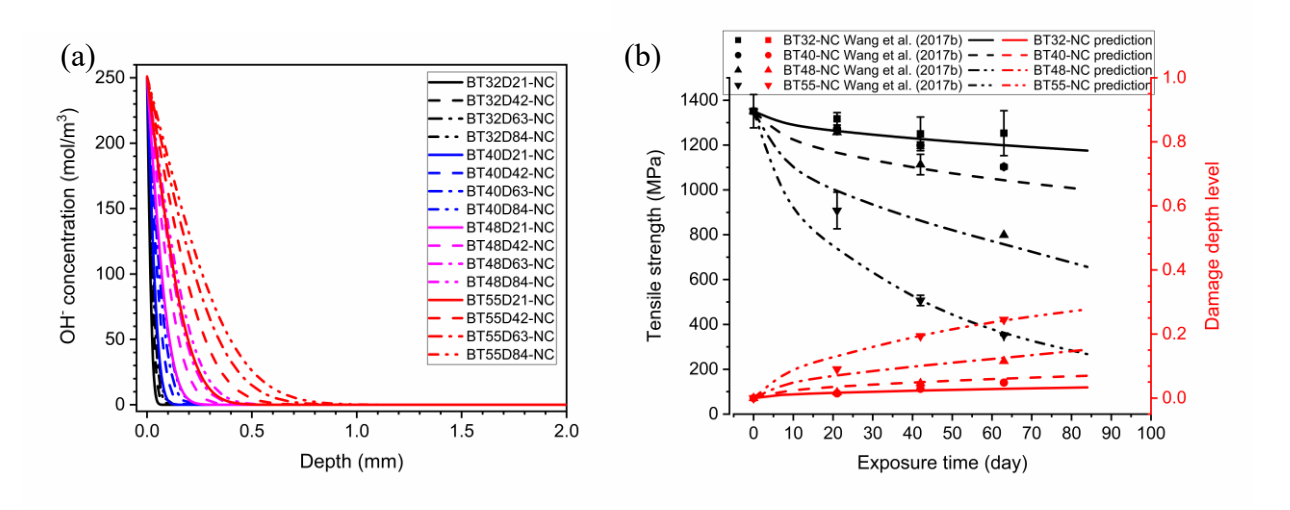


Fig. 6 Predicted results of (a) OH⁻ concentration and (b) tensile strength of BFRP bars in NC SWSSC pore solution Note: BT32D21 represents the conditioned BFRP bars with an exposure period of 21 days at 32°C. B denotes the basalt fiber, T denotes temperature, D denotes the exposure days. NC denotes the normal concrete pore solution.

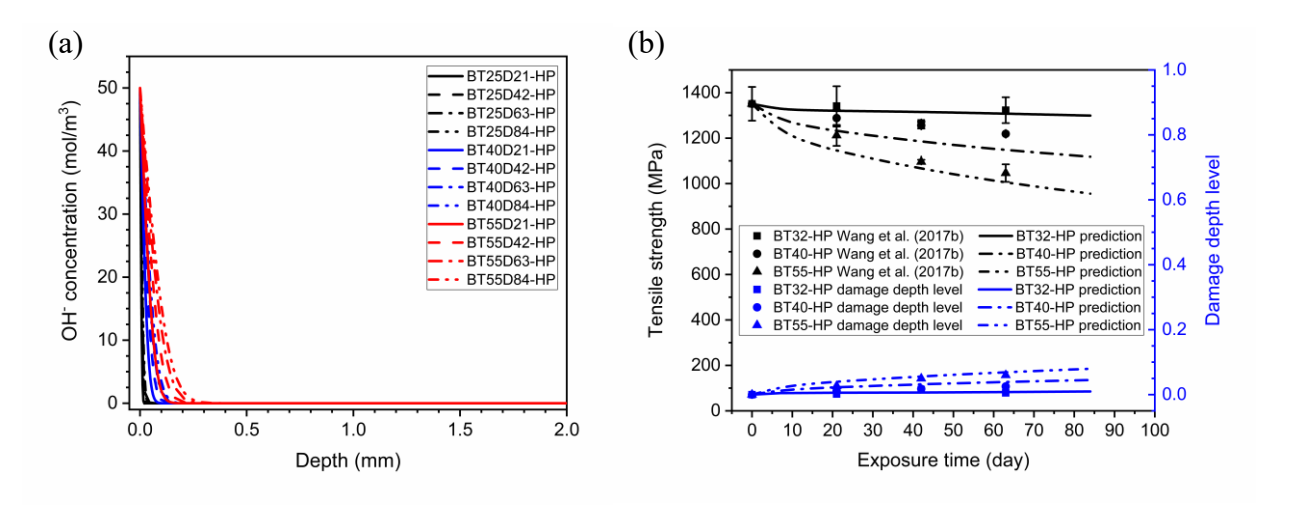


Fig. 7 Predicted results of (a) OH⁻ concentration and (b) tensile strength of BFRP bars in HP SWSSC pore solution Note: BT55D84 represents the conditioned BFRP bars with an exposure period of 84 days at 55°C. B denotes the basalt fiber, T denotes temperature, D denotes the exposure days. HP denotes the high-performance concrete pore solution.

3.2 Pultruded CFRP bars

The shear strength degradation of pultruded CFRP bars under normal concrete (NC) and high-performance (HP) seawater sea-sand concrete (SWSSC) pore solutions (Wang et al., 2017a) was adopted to verify the accuracy of HIDM. The predicted shear strength was compared with experimental

326 and four exposure durations (21, 42, 63, 84 days) in both NC and HP pore solutions, with pH levels of 327 13.4 and 12.7, respectively. 328 The OH⁻ concentration distributions in CFRP bars after exposure are depicted in Figs. 8(a) and 9(a). 329 The results show that increased temperatures accelerated the diffusion processes, significantly 330 increasing the damage depth of the CFRP bars. Consequently, shear strength decreased with increasing 331 temperature and exposure time in both NC and HP SWSSC pore solutions, as shown in Figs. 8(b) and 332 9(b). 333 The shear values of CFRP bars predicted by HIDM closely matched the experimental results when 334 the CFRP bars retained high strength (greater than 75%). For instance, the maximum RE between 335 predictions and experimental data was only 4.8% when the retentions were greater than 75% in both 336 NC and HP SWSSC solutions, as indicated in Figs. 8(b), 9(b). The test results for conditions T55D42 and T55D63 were excluded due to inconsistencies likely caused by low manufacturing quality. 337 338 However, the REs increased when the CFRP bars lost most of their strength (e.g., approximately 50% 339 strength loss). Prediction accuracy becomes more influenced by manufacture defects as the intact area 340 of CFRP bars diminishes. Normal diffusion paths may be altered due to voids, holes, and regional 341 defects in the cross-section, reducing the effective radius of bars and the intact thickness of FRP 342 laminates or tubes as temperature and exposure time increase. Additionally, FRP bars, laminates, and 343 tubes lose their service functions when the damage depth became large, significantly degrading bond 344 strength with adjacent concrete. Therefore, predicting the mechanical strength of FRP composites loses 345 engineering significance under severe degradation conditions.

data across 24 exposure conditions, comprising combinations of three temperatures (25°C, 40°C, 55°C)

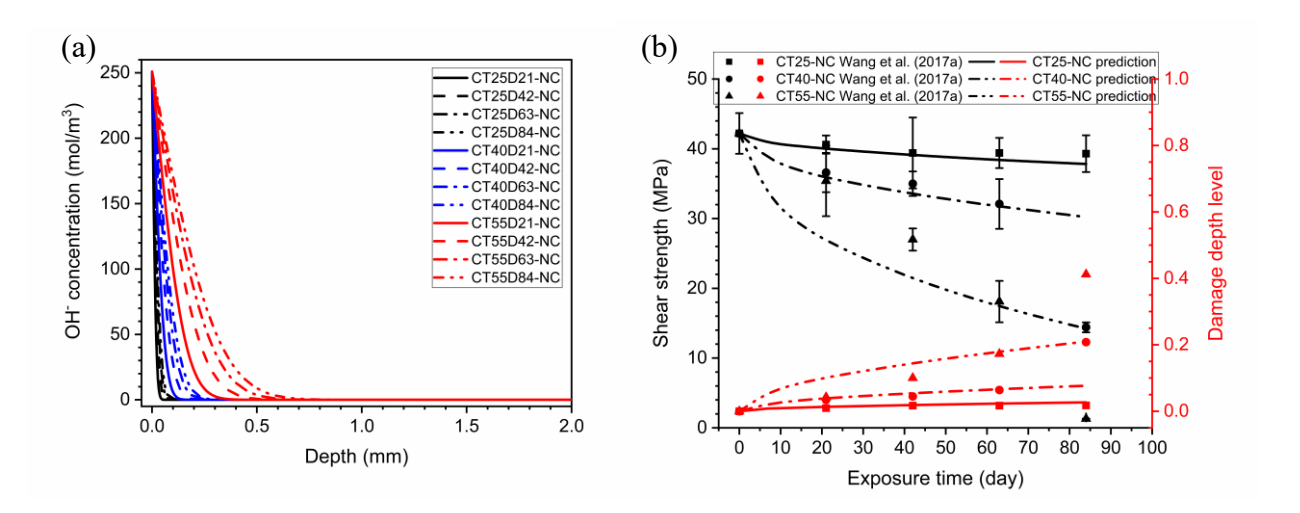


Fig. 8 Predicted results of (a) OH⁻ concentration and (b) tensile strength of CFRP bars in NC SWSSC pore solution Note: CT25D21 represents the conditioned CFRP bars with an exposure period of 21 days at 25°C. C denotes the carbon fiber, T denotes temperature, D denotes the exposure days. NC denotes the normal concrete pore solution.

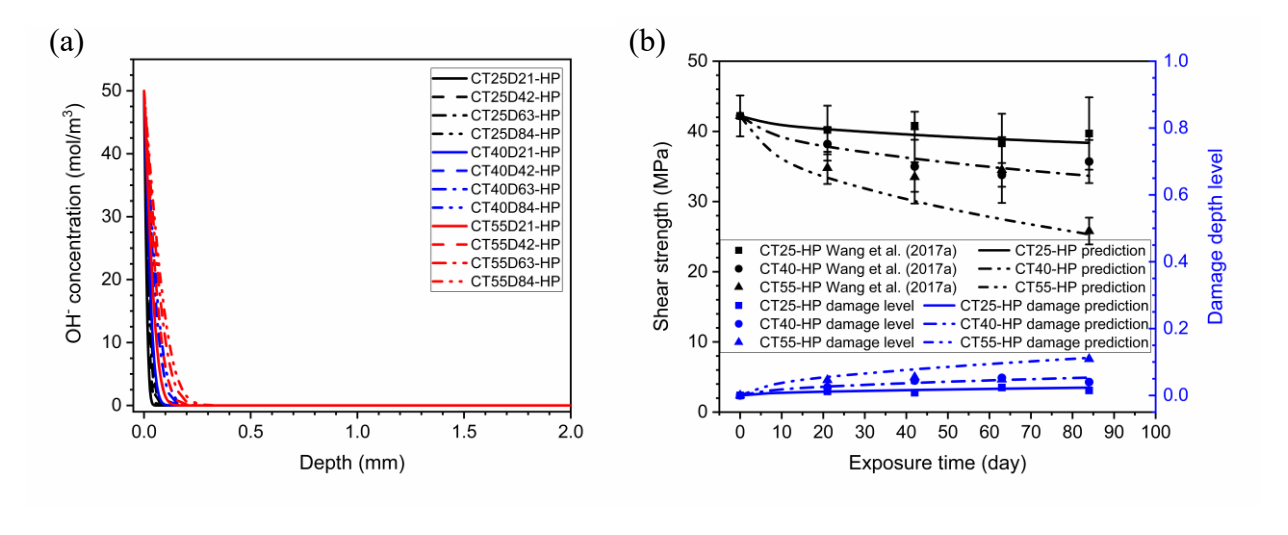


Fig. 9 Predicted results of (a) OH⁻ concentration and (b) tensile strength of CFRP bars in HP SWSSC pore solution

Note: CT55D84 represents the conditioned CFRP bars with an exposure period of 84 days at 55°C. C denotes the carbon fiber, T denotes temperature, D denotes the exposure days. HP denotes the high-performance concrete pore solution.

3.3 Pultruded GFRP bars

The shear strength of pultruded GFRP bars under normal concrete (NC) and high-performance (HP) seawater sea-sand concrete (SWSSC) environments (Wang et al., 2017a) was evaluated to verify the prediction accuracy of HIDM. As mentioned in the two cases above, the accelerated tests involved

three temperatures (25°C, 40°C, 55°C) and four exposure durations (21, 42, 63, and 84 days) in the NC and HP SWSSC pore solutions.

The predictions of OH⁻ distributions and the resultant shear strength are illustrated in Figs. 10(a) and 11(a). The predicted shear strength of GFRP bars in HP SWSSC pore solutions was notably accurate, as shown in Fig. 11(b). All predictions had a maximum RE of 4.6%, except for the condition T40D21, where the RE was 7%. The RE between the experimental and predicted shear strength in the NC SWSSC environment varied from 1.1% - 8.8% when the retentions remained higher than 75%. Despite the wide dispersion of experimental data due to manufacturing and testing variability, the predicted results provided by HIDM are still acceptable.

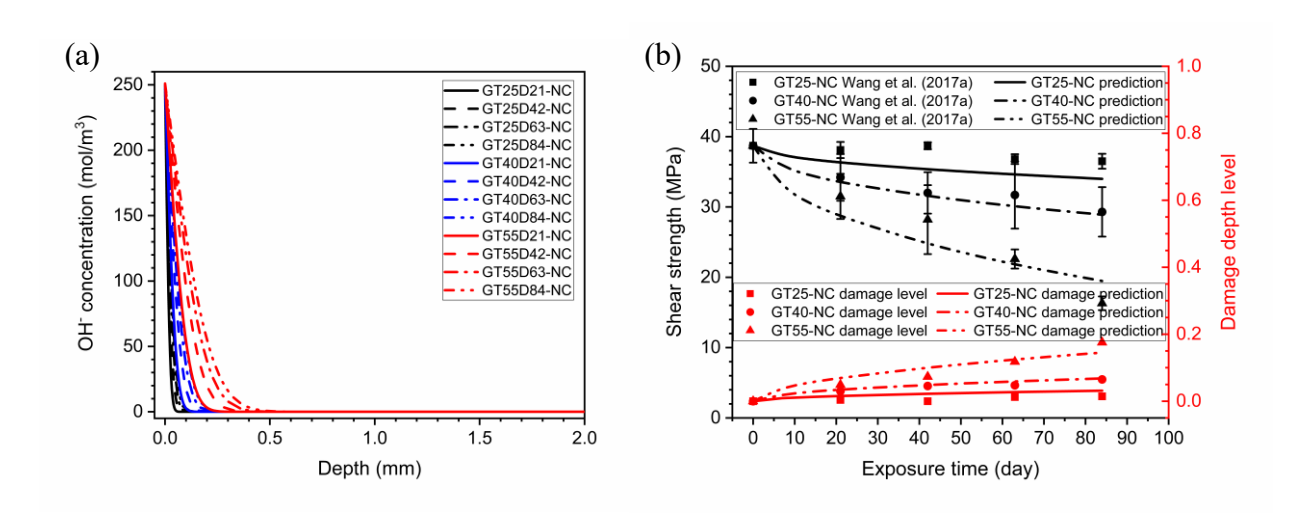


Fig. 10 Predicted results of (a) OH⁻ concentration and (b) tensile strength of GFRP bars in NC SWSSC pore solution

Note: GT25D21 represents the conditioned GFRP bars with an exposure period of 21 days at 25°C. G denotes the glass fiber, T denotes temperature, D denotes the exposure days. NC denotes the normal concrete pore solution.

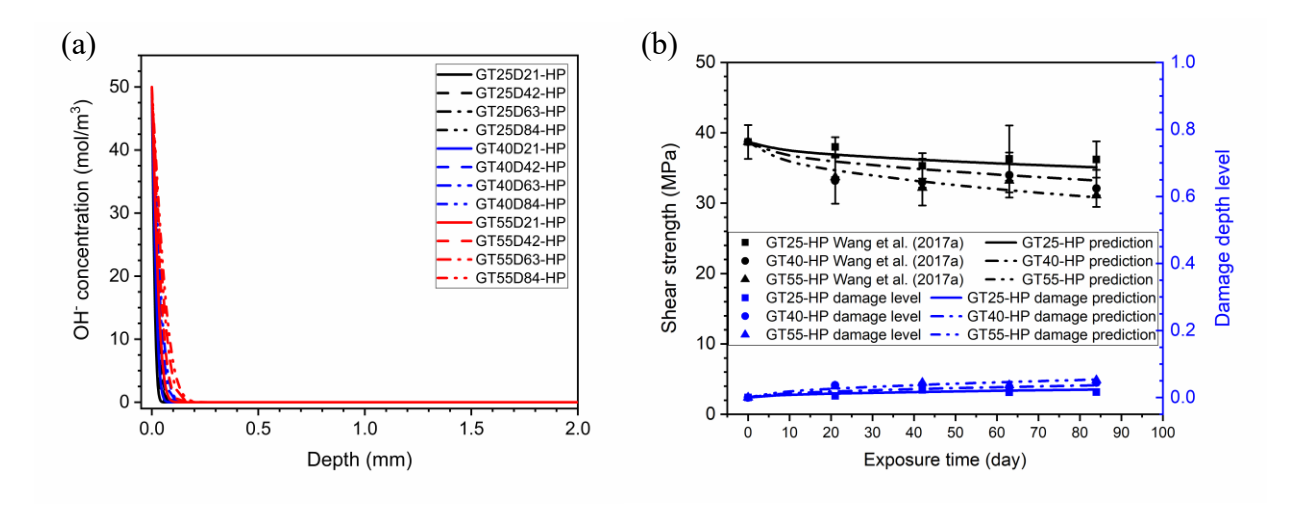


Fig. 11 Predicted results of (a) OH⁻ concentration and (b) tensile strength of GFRP bars in HP SWSSC pore solution

Note: GT25D21 represents the conditioned GFRP bars with an exposure period of 21 days at 25°C. G denotes the glass fiber, T denotes temperature, D denotes the exposure days. HP denotes the high-performance concrete pore solution.

3.4 Pultruded BFRP laminates

The tensile strength of pultruded BFRP laminates in alkaline solutions (Wang et al., 2020) was used to identify the applicability of HIDM for FRP composites with various cross-sectional shapes. The BFRP laminates were immersed in an alkaline solution with a pH of 13.0 at 60°C for 7, 14 30, 90, and 180 days.

Considering the 1D diffusion process in the cross section of FRP laminates, the damage depth was calculated using Eqs. (9) and (10). The predicted strength was then compared to the experimental results, as illustrated in Fig. 12. The predictions closely matched the experimental results when the tensile strength retentions were greater than 60%, with a maximum RE of 4.8%. However, the prediction accuracy decreased when the tensile strength retentions decreased sharply below 60%.

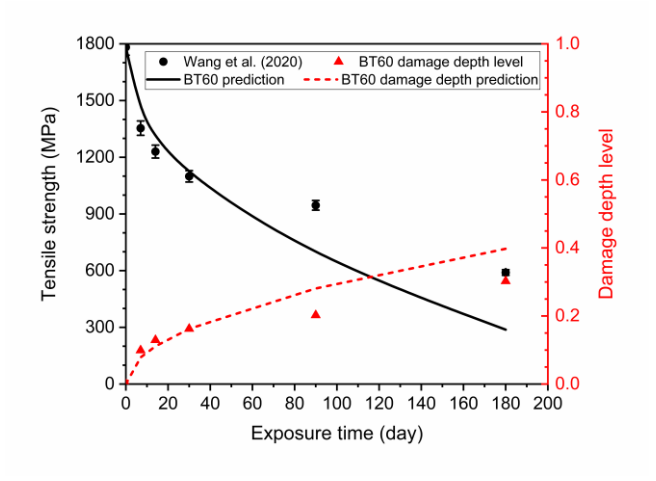
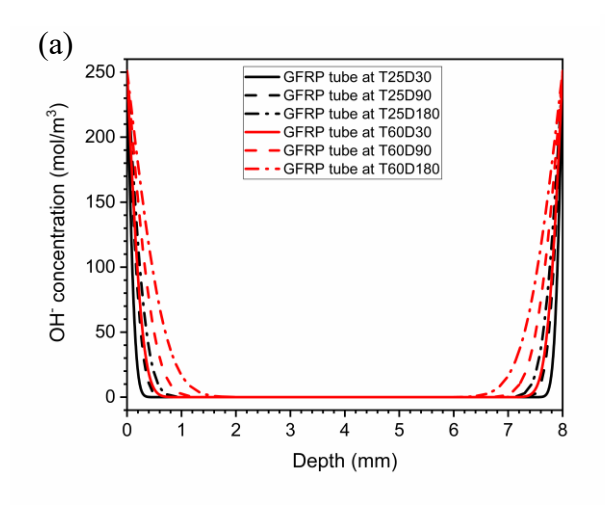


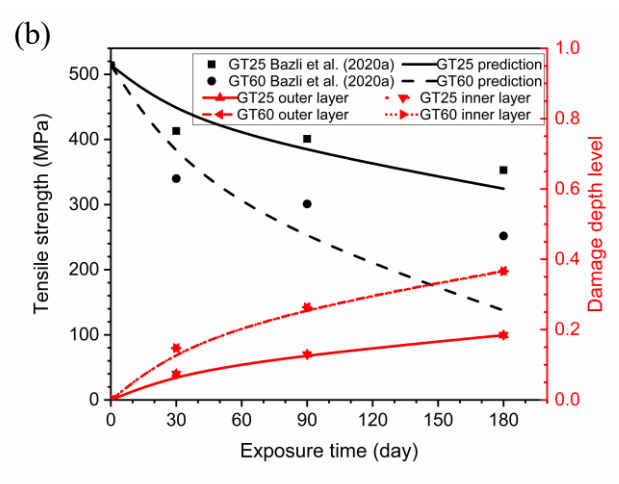
Fig. 12 Predicted results of BFRP laminates in concrete pore solution

Note: BT60 represents the conditioned BFRP laminate under exposure at 60°C.

3.5 Pultruded GFRP tubes

The tensile strength data of pultruded GFRP tubes with a thickness of 8 mm from Bazli et al. (Bazli et al., 2020a) were selected to compare with the predictions from HIDM. The GFRP tubes were exposed to the SWSSC pore solutions with the pH values of 13.4 at 25°C and 60°C for 30, 90, and 180 days (termed as T25D30, T25D90 and T25D180; T60D30, T60D90, and T60D180), respectively. It is important to note that the diffusion of OH ions developed from both the outer and inner surfaces of the GFRP tubes. Therefore, the damage depths on both surfaces were calculated. The OH distributions and predicted tensile strengths are illustrated in Fig. 13(a). Where compared to the test data, the predicted tensile strength values at 25°C and 60°C were acceptable, especially when the strength retention were higher than 70%, with a maximum RE of 4.8%, as shown in Fig. 13(b).





3.6 I-shaped and U-shaped Pultruded GFRP profiles

I-shaped and U-shaped pultruded GFRP profiles were used to verify the applicability of HIDM for FRP profiles with complex cross-sectional types. Generally, FRP composites with intricate cross-sections can be considered as combinations of FRP laminates/plates, circular shapes, and tubes. For instance, the I-shaped and U-shaped pultruded GFRP profiles illustrated in Fig. 14 consist of one web plate and two flange plates. When FRP profiles were immersed into SWSSC pore solution, the OH distributions in each part (i.e., web and flange laminates/plates) of the I-shaped and U-shaped FRP composites can be calculated using Eq. (9). Subsequently, the diffusion depth (R_{df}) can be determined according to Eqs. (15) and (18). Here, due to the negligible effects of OH variations near the plate edges on the total corroded areas, 1D diffusion was used to calculate the diffusion depth.

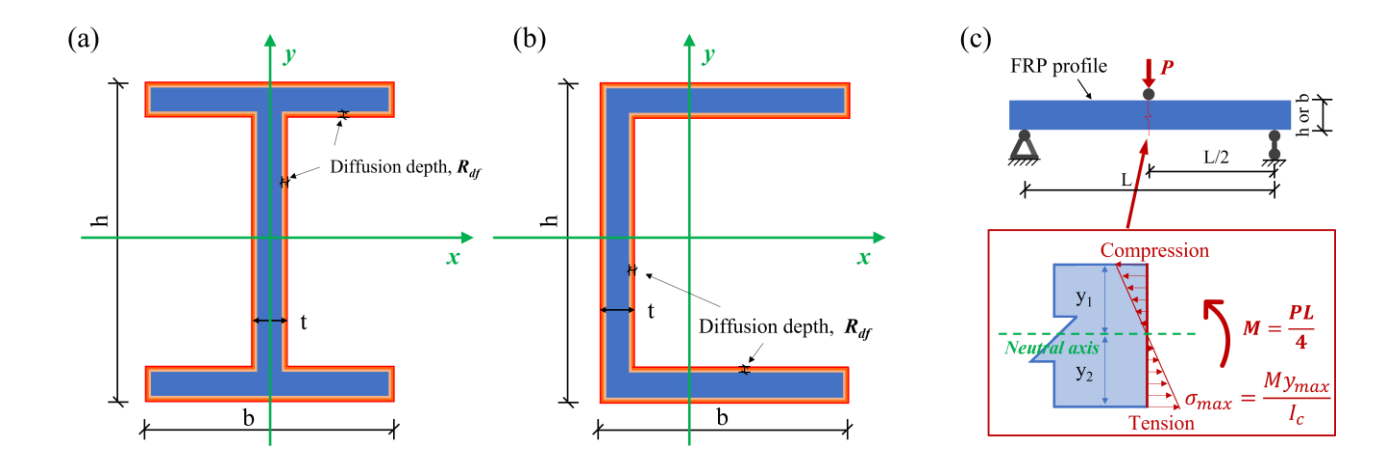


Fig. 14 FRP profiles with cross-sections of (a) I-shape and (b) U-shape; (c) three-point bending test

As illustrated in Fig. 14(c), three-point bending tests can be used to evaluate the bending strength

degradation of FRP profiles with complex cross-sections before and after exposure. The ultimate

bending capacity of these profiles decreased due to the reduced cross-sectional area, as illustrated in

Fig. 14 (a) and (b). Based on the maximum stress criteria, the ultimate stress in both intact and exposed FRP profiles under bending remained unchanged. Therefore, we have

$$\frac{P_t}{P_0} = \frac{I_t}{I_c} \cdot \frac{y_0}{y_t} \tag{21}$$

where P_t and P_0 denote the ultimate force applied at mid-span (see Fig. 14 (c)) for exposed and reference FRP profiles, respectively, under bending tests after a given exposure time t. I_t is the effective moment of inertia of the exposed FRP beam's cross-section, while I_c is the moment of inertia of the reference FRP beam's cross-section. y_t and y_0 are the maximum distances from the edge to the neutral axis for the exposed and reference FRP beams, respectively.

The GFRP laminate, along with I-shaped and U-shaped (channel) vinyl-based GFRP profiles with different cross-sections, were immersed in SWSSC pore solution for 90 days (Bazli et al., 2020). After exposure, three-point bending tests were performed on these specimens, and the results were compared with control GFRP specimens, as illustrated in Fig. 14. It is noteworthy that all profiles used the same

exposure, three-point bending tests were performed on these specimens, and the results were compared with control GFRP specimens, as illustrated in Fig. 14. It is noteworthy that all profiles used the same fibers, matrices, mixture proportions, and manufacturing processes. The experimental results (Bazli, Zhao, Jafari, et al., 2020) were used to validate the applicability of the HIDM model for GFRP profiles with various cross-sectional configurations. The diffusion depth of the GFRP laminate after 90 days of exposure was calculated using Eq. (18). Since diffusion occurs from both sides of the GFRP laminate and the diffusion is negligible compared to the laminate thickness, the total diffusion depth R_{df} can be treated as twice the one-side diffusion depth of OH⁻ ions.

The prediction results of the I-shaped and U-shaped GFRP profiles using HIDM agreed well with experimental data, as shown in Fig. 15 and Table 6. For example, after 90 days of exposure to SWSSC pore solution, the predicted bending strength retentions of the I-shaped specimen I1 and U-shaped

442

443

444

445

446

447

448 449

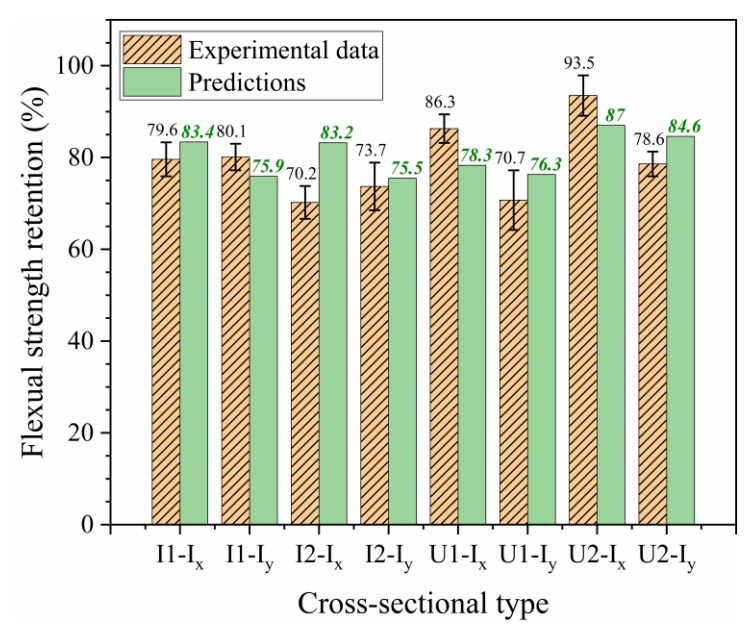


Fig. 15 Validations of I-shaped and U-shaped GFRP profiles using HIDM

Table 6 Comparative results of I-shaped and U-shaped GFRP profiles after 90 days of exposure

Cross-section type	Specimen	Cross-	-section	al size	I_{c}	y_0	Exper	imen	tal data			Predicted	l values	RE
		h	b	t	(mm ⁴)	(mm)	Max load	CV	Retention	It	Уt	Max load	Retention	(%)
		(mm)	(mm)	(mm)			P ₀ (N)	(%)	(%)	(mm ⁴)	(mm)	$P_{t}(N)$	(%)	
I-shape (I1)	Control	25.5	15.0	4.0	15814	12.8	6292	0.8	100					
Major axis (I _x)	Exposed	24.8	14.3	3.3			5012	3.7	79.6	12843	12.4	5245	83.4	3.8
I-shape (I1)	Control	25.5	15.0	4.0	2343	7.5	3203	1.0	100					
Minor axis (I _y)	Exposed	24.8	14.3	3.3			2565	2.9	80.1	1701	7.2	2432	75.9	4.2
I-shape (I2)	Control	38.3	15.0	4.0	44727	19.2	10793	2.2	100					
Major axis (Ix)	Exposed	37.6	14.3	3.3			7578	3.6	70.2	36572	18.8	8979	83.2	13

I-shape (I2)	Control	38.3	15	4	2412	7.5	6577	1.26	100				
Minor axis (I _y)	Exposed	37.6	14.3	3.3			4853	5.2	73.7	1741 7.1	5 4966	75.5	1.8
U-shape (U1)	Control	50	30	3	120836	25	4320	2.25	100				
Major axis (I _x)	Exposed	49.3	29.3	2.3			3727	3.12	86.3	93428 24.	67 3385	78.3	8.0
U-shape (U1)	Control	50	30	3	27478	10.36	7250	0.9	100				
Minor axis (I _y)	Exposed	49.3	29.3	2.3			5131	6.5	70.7	20753 10	25 5531	76.3	5.6
U-shape (U2)	Control	50	30	5	179167	25	7659	1.89	100				
Major axis (I _x)	Exposed	49.3	29.3	4.3			7161	4.4	93.5	153791 24.	67 6662	87.0	6.5
U-shape (U2)	Control	50	30	5	41667	10	11002	1.1	100				
Minor axis (I _y)	Exposed	49.3	29.3	4.3			8658	2.7	78.6	34873 9.8	39 9307	84.6	6.0

4 Conclusion remarks

In this paper, the degradation mechanisms of pultruded FRP composites with various types of fibers and matrices under concrete environments are summarized. The fibers include basalt, carbon, and glass fibers, while the polymer matrices comprise the amine-cured and anhydride-cured epoxy, vinyl ester, and unsaturated polyester. The damage mechanisms of the FRP constitutions are identified and classified into three groups. Based on their damage mechanisms, a physically based generalized degradation model, the hydroxyl ions diffusion-based model (HIDM) proposed by the authors, is validated using the available test data from published literature. The HIDM demonstrates good accuracy when the FRP composites retain adequate strength to reinforce concrete, specifically with a strength retention of greater than 70%. Besides, the damage depth level is proposed for the bond failure analysis of FRP bar-concrete structures, providing a quantitative parameter and unique perspective to the current codes. The following conclusions can be drawn:

- Both basalt and glass fibers can be etched and leached under concrete environments (i.e., alkaline
 or salt-alkaline pore solutions), whereas carbon fibers are inert to these corrosive environments.
 The degradation of the interface between fibers and matrix is similar to the etching of glass fibers.
- Unsaturated polyester, styrene-cured vinyl ester, and anhydride-cured epoxy matrices can be significantly damaged by hydrolysis in alkaline environments. The degradation of amine-cured epoxy matrices under alkaline solutions usually originates from water uptake and the resultant swelling, along with the dissociation of secondary/tertiary amines and ethers in the amine-cured

471 epoxy.

- The degradation of pultruded FRP composites under alkaline solutions can be predicted by the generalized degradation model, HIDM, regardless of the shapes of FRP composites, such as bars, tubes, and sections. The generalized degradation model is proposed based on exposure to pore solutions, and its application in relative humidity environment are still needed using a shift equation, i.e., liquid-gas-state shift theory (Zhao, Iwama, et al., 2024), which will be present in our following research.
 - The structural safety of FRP-reinforced concrete structures will be significantly weakened when the damage depth became greater than 6% diameter of FRP bars, corresponding to a strength retention of 77.4%. Consequently, the bond strength between FRP bars and concrete can no longer be guaranteed.
 - The proposed FRP bar-to-concrete bond failure criteria define a quantitative parameter to evaluate the bonding conditions of FRP bar-concrete structures as service time increases, providing insights and new perspective to the current design guides. It should be noted that the 6% criterion is derived from limited rib-geometry reported in Zhang et al. (2024b,c). Future work is needed to derive a more general criterion to cover different surface treatments, embedment lengths, or concrete strengths.

Appendix

Table A1 Diffusion coefficients of FRP composites used in the validation

Data source	FRP type	Exposure environment	Temperature	Diffusion coefficient
				(mm^2/s)
Wu et al. (Wu et al., 2015)	BFRP bars	Concrete pore solution with a pH	25°C	5.26×10 ⁻¹¹
		value of 13.0	40°C	2.49×10 ⁻¹⁰
			55°C	1.02×10 ⁻⁹
Wang et al. (Wang et al., 2017b)	BFRP bars	Seawater sea-sand concrete pore	32°C	9.86×10 ⁻¹¹
		solution with a pH value of 13.4	40°C	4.46×10 ⁻¹⁰
			48°C	1.87×10 ⁻⁹
			55°C	6.20×10 ⁻⁹
Wang et al. (Wang et al., 2017b)	BFRP bars	Seawater sea-sand concrete pore	32°C	1.06×10^{-10}
		solution with a pH value of 12.7	40°C	2.06×10 ⁻¹⁰
			55°C	6.52×10 ⁻¹⁰

Wang et al. (Wang, Zhao, Xian,	CFRP bars	Seawater sea-sand concrete pore	25°C	6.26×10 ⁻¹¹
Wu, Singh Raman and Al-Saadi,		solution with a pH value of 13.4	40°C	5.36×10 ⁻¹⁰
2017)			55°C	3.77×10 ⁻⁹
Wang et al. (Wang, Zhao, Xian,	CFRP bars	Seawater sea-sand concrete pore	25°C	5.56×10 ⁻¹¹
Wu, Singh Raman and Al-Saadi,		solution with a pH value of 12.7	40°C	2.89×10 ⁻¹⁰
2017)			55°C	1.29×10 ⁻⁹
Wang et al. (Wang, Zhao, Xian,	GFRP bars	Seawater sea-sand concrete pore	25°C	8.65×10 ⁻¹¹
Wu, Singh Raman and Al-Saadi,		solution with a pH value of 13.4	40°C	4.21×10 ⁻¹⁰
2017)			55°C	1.77×10 ⁻⁹
Wang et al. (Wang, Zhao, Xian,	GFRP bars	Seawater sea-sand concrete pore	25°C	5.84×10 ⁻¹¹
Wu, Singh Raman and Al-Saadi,		solution with a pH value of 12.7	40°C	1.36×10 ⁻¹⁰
2017)			55°C	2.93×10 ⁻¹⁰
Wang et al. (Wang et al., 2020)	BFRP laminates	Alkaline solution with a pH value	60°C	3.60×10 ⁻⁹
		of 13.0		
Bazli et al. (Bazli, Zhao, Bai, et	GFRP tubes	Seawater sea-sand concrete pore	25°C	2.5×10 ⁻⁹
al., 2020)		solution with a pH value of 13.4	60°C	9.6×10 ⁻⁹

CRediT authorship contribution statement

Qi Zhao: Conceptualization, Data curation, Formal analysis, Investigation, Methodology, Project administration, Software, Validation, Visualization, Writing — original draft. Daxu Zhang: Conceptualization, Methodology, Writing — review & editing. Jie Liu: Methodology, Formal analysis, Investigation, Writing — review & editing. Keitai Iwama: Methodology, Writing — review & editing. Pei-Fu Zhang: Methodology, Writing — review & editing. Lingxin Zeng: Methodology, Writing — review & editing. Xiao-Ling Zhao: Conceptualization, Methodology, Project administration, Resources, Supervision, Writing — review & editing.

Acknowledgements

490

491

492

493

494

495

496

497

498

499

503

504

The first author is sponsored by the Innovation and Technology Fund (ITF) Research Talent Hub of Hong Kong. The study is supported by the Henan Province Science and Technology Research Projects (242102320013).

Declaration of competing interest

The authors declare that they do not have any commercial or associative interest that represents a

505 conflict of interest in connection with the work submitted. 506 Data availability 507 Data will be made available on request from corresponding author. 508 Declaration of generative AI in scientific writing 509 The authors declare that any generative AI was not used in preparation of the work submitted. 510 511 References 512 ACI Committee 440 (2015) Guide for the Design and Construction of Concrete Reinforced with FRP 513 Bars (ACI 440.1R-15). Farmington Hills, MI: American Concrete Institute. 514 ACI Committee 440 (2017) Guide for the Design and Construction of Externally Bonded FRP 515 Systems for Strengthening Concrete Structures (ACI 440.2R-17). Farmington Hill, MI: 516 American Concrete Institute. 517 ACI Committee 440 (2023) Building Code Requirements for Structural Concrete Reinforced with 518 Glass Fiber-Reinforced Polymer (GFRP) Bars-Code and Commentary (ACI 440.11-22). 519 Farmington Hills, MI: American Concrete Institute. 520 Allen DG and Atadero RA (2012) Evaluating the Long-Term Durability of Externally Bonded FRP 521 via Field Assessments. Journal of Composites for Construction 16(6): 737–746. 522 Antoon MK and Koenig JL (1980) The Structure and Moisture Stability of the Matrix Phase in 523 Glass-Reinforced Epoxy Composites. Journal of Macromolecular Science, Part C 19(1): 135– 524 173. 525 Arias JPM, Bernal C, Vázquez A, et al. (2018) Aging in Water and in an Alkaline Medium of 526 Unsaturated Polyester and Epoxy Resins: Experimental Study and Modeling. Advances in 527 Polymer Technology 37(2): 450-460. 528 Bazli M, Zhao XL, Bai Y, et al. (2020) Durability of pultruded GFRP tubes subjected to seawater sea 529 sand concrete and seawater environments. Construction and Building Materials 245: 118399. 530 Bazli M, Zhao XL, Jafari A, et al. (2020) Mechanical properties of pultruded GFRP profiles under 531 seawater sea sand concrete environment coupled with UV radiation and moisture. Construction 532 and Building Materials 258: 120369. 533 Bazli M, Zhao XL, Jafari A, et al. (2021) Durability of glass-fibre-reinforced polymer composites 534 under seawater and sea-sand concrete coupled with harsh outdoor environments. Advances in 535 Structural Engineering 24(6): 1090–1109. Benmokrane B., Hassan M, Robert M, et al. (2020) Effect of Different Constituent Fiber, Resin, and 536 537 Sizing Combinations on Alkaline Resistance of Basalt, Carbon, and Glass FRP Bars. *Journal of* 538 Composites for Construction 24(3): 1–18. 539 Benmokrane Brahim, Brown VL, Ali AH, et al. (2020) Reconsideration of the Environmental

Reduction Factor CE for GFRP Reinforcing Bars in Concrete Structures. Journal of Composites

- 541 *for Construction* 24(4): 1–6.
- Brand S, Veith L, Baier R, et al. (2020) New methodical approaches for the investigation of
- weathered epoxy resins used for corrosion protection of steel constructions. *Journal of Hazardous Materials* 395: 122289.
- 545 CEN/TS 19101 (2022) Design of fibre-polymer composite structures.
- Ceroni F, Bonati A, Galimberti V, et al. (2018) Effects of Environmental Conditioning on the Bond Behavior of FRP and FRCM Systems Applied to Concrete Elements. *Journal of Engineering*
- 548 *Mechanics* 144(1): 1–15.
- 549 Chen Y, Davalos JF and Ray I (2006) Durability Prediction for GFRP Reinforcing Bars Using Short-
- Term Data of Accelerated Aging Tests. *Journal of Composites for Construction* 10(4): 279–286.
- 552 Chen Y, Davalos JF, Ray I, et al. (2007) Accelerated aging tests for evaluations of durability
- 553 performance of FRP reinforcing bars for concrete structures. *Composite Structures* 78(1): 101–554 111.
- Chin JW, Aouadi K, Haight MR, et al. (2001) Effects of water, salt solution and simulated concrete
- pore solution on the properties of composite matrix resins used in civil engineering applications.
- 557 *Polymer Composites* 22(2): 282–297.
- 558 Correia JR, Keller T, Garrido M, et al. (2023) Mechanical properties of FRP materials at elevated
- temperature Definition of a temperature conversion factor for design in service conditions.
- 560 *Construction and Building Materials* 367(January).
- Dhondy T, Xiang Y, Yu T, et al. (2021) Effects of mixing water salinity on the properties of
- 562 concrete. Advances in Structural Engineering 24(6): 1150–1160.
- Du Y, Zhang D, Zhang Y, et al. (2024) Predicting tensile behaviour of plain weave CMCs using a
- nonlinear data-driven constitutive model for fibre tow composites. *Ceramics International* 50(9): 16142–16154.
- Fang W and Guo W (2023) Deterioration mechanism of hydrothermal aging on the properties of
- 567 carbon fiber/epoxy composites in various media. *Journal of Composite Materials* 57(7): 1235–568 1246.
- Gao M, Wang J, Zhou Y, et al. (2020) The performance of epoxy coatings containing polyaniline
- (PANI) nanowires in neutral salt, alkaline, and acidic aqueous media. *Journal of Applied*
- 571 *Polymer Science* 137(36).
- Gooranorimi O and Nanni A (2017) GFRP Reinforcement in Concrete after 15 Years of Service.
- *Journal of Composites for Construction* 21(5): 04017024.
- Guo F, Al-Saadi S, Singh Raman RK, et al. (2022) Durability of Fibre Reinforced Polymers in
- Exposure to Dual Environment of Seawater Sea Sand Concrete and Seawater. *Materials* 15(14).
- Hojo H, Tsuda K and Ogasawara K (1991) Form and rate of corrosion of corrosion-resistant FRP
- resins. *Advanced Composite Materials* 1(1): 55–67.
- Hojo H, Tsuda K, Kubouchi M, et al. (1998) Corrosion of plastics and composites in chemical
- environments. *Metals and Materials International* 4(6): 1191–1197.
- Huang J and Aboutaha R (2010) Environmental Reduction Factors for GFRP Bars Used as Concrete
- Reinforcement: New Scientific Approach. *Journal of Composites for Construction* 14(5): 479–
- 582 486.

- Kaushik SK and Islam S (1995) Suitability of sea water for mixing structural concrete exposed to a marine environment. *Cement and Concrete Composites* 17(3): 177–185.
- Kootsookos A and Mouritz AP (2004) Seawater durability of glass- and carbon-polymer composites.

 Composites Science and Technology 64(10–11): 1503–1511.
- Li J, Xie J, Liu F, et al. (2019) A critical review and assessment for FRP-concrete bond systems with epoxy resin exposed to chloride environments. *Composite Structures* 229(100).
- Li YL, Zhao XL and Raman RS (2021) Durability of seawater and sea sand concrete and seawater and sea sand concrete—filled fibre-reinforced polymer/stainless steel tubular stub columns. *Advances in Structural Engineering* 24(6): 1074–1089.
- Liao JJ, Zeng JJ, Bai YL, et al. (2022) Bond strength of GFRP bars to high strength and ultra-high strength fiber reinforced seawater sea-sand concrete (SSC). *Composite Structures* 281(August 2021).
- Lim JSK, Gan CL and Hu XM (2019) Unraveling the Mechanistic Origins of Epoxy Degradation in
 Acids. ACS Omega 4(6): 10799–10808.
- Liu J, Wei Y, Zhao Q, et al. (2024) Fatigue-induced fracture assessment for FRP-steel bonding joints after seawater exposure. *Structures* 68(August).
- Liu Q feng, Hu Z, Wang X er, et al. (2022) Numerical study on cracking and its effect on chloride transport in concrete subjected to external load. *Construction and Building Materials* 325: 126797.
- Long Y, Bai L, Liu L, et al. (2023) Association between Serviceability and Recyclability of Amine-Cured Epoxy Thermosets. *ACS Sustainable Chemistry and Engineering* 11(34): 12790–12797.
- 604 Lu Z, Li Y and Xie J (2021) Durability of BFRP bars wrapped in seawater sea sand concrete.
 605 *Composite Structures* 255(100): 112935.
- Ma Y, Kim D and Nutt SR (2017) Chemical treatment for dissolution of amine-cured epoxies at atmospheric pressure. *Polymer Degradation and Stability* 146(April): 240–249.
- Mallick PK (2018) Processing of Polymer Matrix Composites. Boca Raton: CRC Press.
- Mehta PK and Monteiro PJM (2014) *Concrete: Microstructure, Properties, and Materials.* 4th Ed. New York: McGraw-Hill Education.
- Myers JJ and Viswanath T (2006) A worldwide survey of environmental reduction factors for Fiber Reinforced Polymers (FRP). *Proceedings of the Structures Congress and Exposition* 2006: 96.
- Ortiz JD, Khedmatgozar Dolati SS, Malla P, et al. (2023) FRP-Reinforced/Strengthened Concrete:
 State-of-the-Art Review on Durability and Mechanical Effects. *Materials* 16(5): 1–30.
- Peebles LH (2018) Carbon Fibers: Formation, Structure, and Properties. Taylor and Francis Press.
- Sembokuya H, Negishi Y, Kubouchi M, et al. (2003) Corrosion Behavior of Epoxy Resin Cured with
 Different Amount of Hardener in Corrosive Solutions. *Materials Science Research International* 9(3): 230–234.
- Shrestha J, Ueda T and Zhang D (2015) Durability of FRP Concrete Bonds and Its Constituent
 Properties under the Influence of Moisture Conditions. *Journal of Materials in Civil* Engineering 27(2): 1–14.
- Sun W, Zheng Y, Zhou L, et al. (2021) A study of the bond behavior of FRP bars in MPC seawater concrete. *Advances in Structural Engineering* 24(6): 1110–1123.
- Taha A and Alnahhal W (2021) Bond durability and service life prediction of BFRP bars to steel

- FRC under aggressive environmental conditions. *Composite Structures* 269(April).
- Tanks J, Arao Y and Kubouchi M (2022) Network-level analysis of damage in amine-crosslinked diglycidyl ether resins degraded by acid. *Express Polymer Letters* 16(5): 488–499.
- Teng JG, Xiang Y, Yu T, et al. (2019) Development and mechanical behaviour of ultra-high-
- performance seawater sea-sand concrete. *Advances in Structural Engineering* 22(14): 3100–3120.
- Wang Y, Zhu W, Zhang X, et al. (2020) Influence of thickness on water absorption and tensile strength of BFRP laminates in water or alkaline solution and a thickness-dependent accelerated ageing method for BFRP laminates. *Applied Sciences (Switzerland)* 10(10).
- Wang Z, Zhao XL, Xian G, Wu G, Singh Raman RK and Al-Saadi S (2017) Durability study on interlaminar shear behaviour of basalt-, glass- and carbon-fibre reinforced polymer (B/G/CFRP) bars in seawater sea sand concrete environment. *Construction and Building Materials* 156: 985–1004.
- Wang Z, Zhao XL, Xian G, Wu G, Singh Raman RK, Al-Saadi S, et al. (2017) Long-term durability of basalt- and glass-fibre reinforced polymer (BFRP/GFRP) bars in seawater and sea sand concrete environment. *Construction and Building Materials* 139: 467–489.
- Wu G, Dong Z-Q, Wang X, et al. (2015) Prediction of Long-Term Performance and Durability of
 BFRP Bars under the Combined Effect of Sustained Load and Corrosive Solutions. *Journal of Composites for Construction* 19(3): 04014058.
- Yang BX, Xie TY, Yu Y, et al. (2022) Mechanical properties and environmental performance of seawater sea-sand self-compacting Concrete. *Advances in Structural Engineering* 25(15): 3114– 3136.
- Zhang K, Zhang Q and Xiao J (2022) Durability of FRP bars and FRP bar reinforced seawater sea sand concrete structures in marine environments. *Construction and Building Materials* 350(June): 128898.
- Zhang K, Xiao J, Hou Y, et al. (2022) Experimental study on carbonation behavior of seawater sea sand recycled aggregate concrete. *Advances in Structural Engineering* 25(5): 927–938.
- Zhang P-F, Zhang D, Zhao Xiao-Ling, et al. (2024) Natural language processing-based deep transfer learning model across diverse tabular datasets for bond strength prediction of composite bars in concrete. *Computer-Aided Civil and Infrastructure Engineering* (July): 1–23.
- Zhang PF, Iqbal M, Zhang D, et al. (2024) Bond strength prediction of FRP bars to seawater sea sand concrete based on ensemble learning models. *Engineering Structures* 302(December 2023).
- Zhang PF, Zhao XL, Zhang D, et al. (2024) Prediction of bond strength and failure mode of FRP
 bars embedded in UHPC or UHPSSC utilising extreme gradient boosting technique. *Composite* Structures 346(June): 118437.
- Zhao Q, Zhao J, Dang J-TT, et al. (2019) Experimental investigation of shear walls using carbon fiber reinforced polymer bars under cyclic lateral loading. *Engineering Structures* 191(April): 82–91.
- Zhao Q, Zhang D, Zhao X-L, et al. (2021) Modelling damage evolution of carbon fiber-reinforced epoxy polymer composites in seawater sea sand concrete environment. *Composites Science and Technology*: 108961.
- Zhao Q, Zhang D, Zhao X, et al. (2022) Experimental and modelling studies on damage evolution of

- 667 epoxy-based GFRP bars in pore solution environment of seawater sea-sand concrete. *China*668 *Civil Engineering Journal* 55(9): 25–41.
- Zhao Q, Zhao X, Zhang D, et al. (2024) Degradation of GFRP Bars with Epoxy and Vinyl Ester
 Matrices in a Marine Concrete Environment: An Experimental Study and Theoretical Modeling.
 Journal of Composites for Construction 28(2).
- Zhao Q, Iwama K, Dai JG, et al. (2024) Deterioration modelling of GFRP-reinforced cement-based
 concrete infrastructure in service under the natural inland atmospheric environment.
 Construction and Building Materials 447(May): 138005.
- Zhao Q, Zhao X-L, Zhang D, et al. (2024) Effects of exposure in seawater sea-sand concrete pore
 solution on fatigue performance of carbon FRP bars. *Composites Science and Technology* 247:
 110418.
- Zhao X, Zhang PF, Zhao Q, et al. (2025) A SHAP algorithm-based prediction of the interlaminar
 shear strength degradation of G/BFRP bars embedded in concrete exposed to marine
 environment. *Case Studies in Construction Materials* 22(April): e04770.
- Zhao X, Zhang PF, Zhang D, et al. (2025) Prediction of interlaminar shear strength retention of FRP bars in marine concrete environments using XGBoost model. *Journal of Building Engineering* 105(June 2024).
- Zhou W, Feng P and Yang JQ (2021) Advances in coral aggregate concrete and its combination with FRP: A state-of-the-art review. *Advances in Structural Engineering* 24(6): 1161–1181.